Takeoff Drag Prediction for Airbus A300-600 and A310 Compared with Flight Test Results

B. Haftmann,* F.-J. Debbeler,† and H. Gielen†
Messerschmitt-Bölkow-Blohm GmbH, Bremen, Federal Republic of Germany

A semiempirical method is described that was applied to predict the preflight drag of the A310 and the A300-600 for takeoff, one-engine conditions. The first part of the present paper is concerned with wind-tunnel models and tests basically designed to obtain aerodynamic performances at low speeds, i.e., drag and maximum lift. In addition, special measurements with turbine-powered simulators (TPS) are described which were performed to investigate the effect of installed engines on second-segment climb drag. The correction of tunnel results to full-scale aircraft data is the subject of the next part. A simple scaling rule is shown covering the effect of Reynolds number on lift, pitching moment, and drag. The quality of this rule is demonstrated by a comparison of scaled results with corresponding model data obtained in a pressurized wind tunnel. The third part of the paper compares flight test results with corresponding predictions for several takeoff configurations. It is demonstrated that with the model/test philosophy and the scaling method described, the predictions agree with the flight test data within a range of ±1% of overall drag.

I. Introduction

THE takeoff performances of transport aircraft are usually defined by second-segment climb requirements where, for twin engine jets, a climb rate of 2.4% with one engine inoperating has to be demonstrated. The bottom portion of Fig. 1 shows this takeoff procedure. The second segment starts with "undercarriage in" and ends 400 ft over ground. During this period, the minimum climb rate of 2.4% has to be demonstrated with an aircraft speed not less than 20% over stall speed. The aircraft drag at these conditions can be split into two parts: 1) the symmetrical portion of the basic configuration, and 2) the asymmetrical portion, which includes one-engine windmill drag and the trim drag due to rudder/aileron deflection. This paper concentrates on the prediction method applied to obtain the symmetrical drag portion.

As shown in the left-hand portion of Fig. 1, the most important contributions are the lift-dependent drag, with approximately 80%, and the shape drag, with approximately 18%. Both portions are R_N dependent, which effect is the subject of this paper.

II. Basic Wind-Tunnel Tests

A. Complete Model Measurements

General Test Requirements

To establish the basic drag level, tunnel tests are needed to provide data of high accuracy and repeatability. Hence, low tunnel flow turbulence, high balance accuracy, model suspensions of low interference, and careful model design are required. Within Airbus Industrie, three particular tunnels are used to get low-speed performances. These are the pressurized facilities Fauga F1, with a test section of 4.5 × 3.5 m; at RAE with a test section of 5 × 5 m; and the atmospheric Deutsch Niederlämdisscher wind tunnel, with a test section of 6 × 8 m. With the method described in this paper, it is of less importance which test Reynolds number is chosen if the flow behavior up to $C_{L1.2Vs}$ is as expected for the aircraft. This means that flow separations that do not exist at full-scale Reynolds numbers have to be avoided either by partial model modifications or by tests at high Reynolds numbers. In any case, before starting performance tests, one has to check the flow behavior around the model.

Model Arrangements and Accuracy

Figures 2 and 3 show the A310 and A300-600 model arrangements in the DNW. Suspension is a single sting combined with an internal strain gage balance. Compared with a three-strut suspension, also shown in the figure, which is usually used in the pressurized tunnels, the single sting provides less interference, but the accuracy of internal balances are usually less than the accuracy of external ones. The main difficulty with internal balances of the size we are talking about is inhomogeneous temperature effects, which are different between installed and laboratory conditions and are therefore not easy to compensate. In very close cooperation with the DNW, these problems have been minimized, and we are now at a long-time repeatability of about ±5 drag counts, which is less than ±0.5% of the total second segment climb drag.

Model Configuration

The basic tests are carried out with the model in tail-off configuration. As shown in Fig. 4, all parts of the model except the wing are provided with carborundum strips to fix the location of the laminar/turbulent boundary-layer transition. This enables the shape drag calculation under consideration of an exact known laminar portion. The strips should be positioned just behind the pressure peaks, and a transition check with

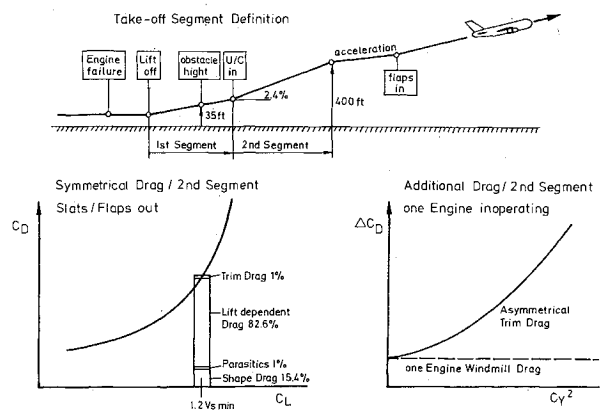

Fig. 1 Takeoff segment definitions and drag portions.

Presented as Paper 86-1.10.1 at the 15th Congress of the International Council of Aeronautical Sciences (ICAS), London, England, Sept. 7-12, 1986; received Dec. 21, 1986; revision received Oct. 25, 1987.

*Chief Aerodynamicist, Civil Aircraft Program.
†Type Aerodynamicist.

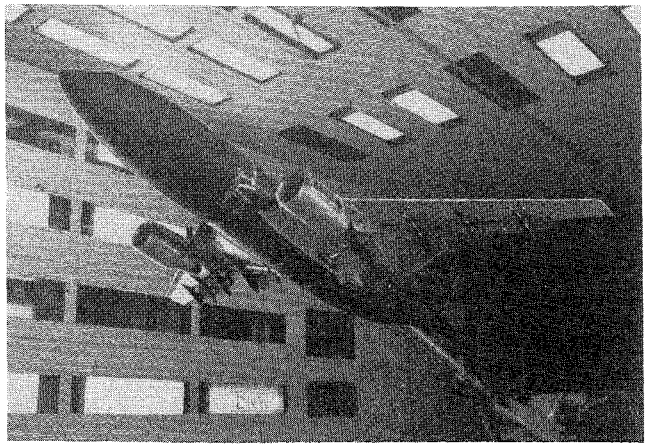

Fig. 2 A310 model arrangement in the DNW.

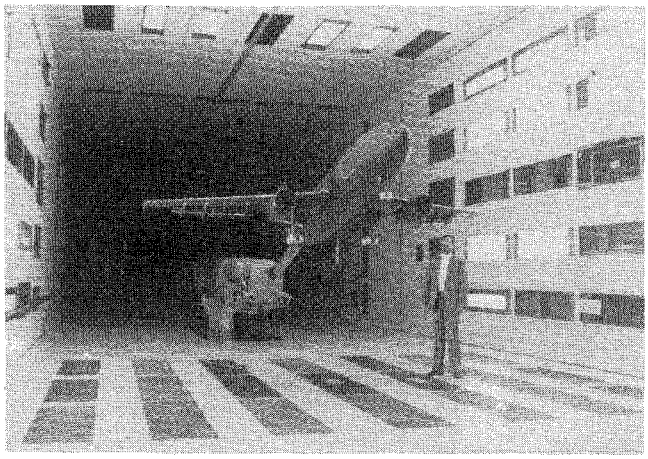

Fig. 3 A300-600 model arrangement in the DNW.

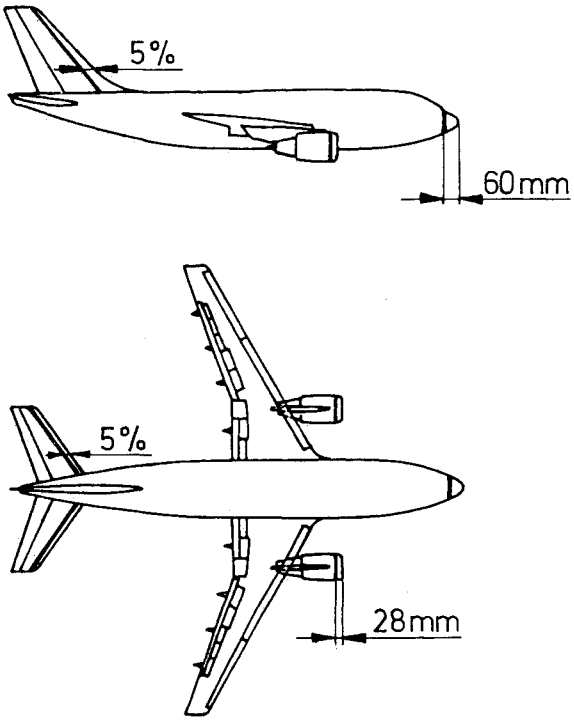

Fig. 4 Transition fixing on A310 models.

china clay or another technique should be carried out before starting force measurements. Table 1 shows the strip positions chosen for A310 and A300-600 models being tested in the DNW. Because of the nature of pressure distribution on the wing with slats deployed, a natural transition at or near the leading edge occurs that makes an artificial promoter unnecessary.

Engine Representation

The engines are generally represented by through-flow nacelles (TFN). As shown in Fig. 4, the CF6-80A is designed as a single-body skirted nacelle extended to the end of the hot gas nozzle. However, this simple design cannot be applied in general, especially if the fan exit plane is close to the wing leading edge. In those cases, it is better to design a double-body nacelle where the interference between fan exit and wing becomes more representative with special respect to maximum lift investigations. The nacelles are designed to provide a mass flow ratio representing the "flight idle" condition of the real engine at Mach = 0.2 and 5000 ft altitude. Figure 5 illustrates this design point within the range of most important engine conditions at low speeds. It can be seen that both A310 engine types, i.e., General Electric and Pratt & Whitney, agree well in absolute values and their development vs Mach number. However, the range of mass flow ratios between windmill and maximum takeoff power is comparably large. The sketches beside the curves give an impression of the corresponding different stream tubes, and it is obvious that the mass flow ratio will influence the overall forces and moments of the aircraft. Tests to obtain these effects will be described later.

Test Conditions

As mentioned before, the Reynolds number does not necessarily influence the final accuracy of the drag assessment. It should, however, not be less than 2×10^6. Mach number should be 0.2 or less. In any case, it is important that the maximum lift does not include Mach effects. Later on it will be shown that the R_N corrections to be applied depend on the ratio of model/full-scale maximum lift, which explains how effects other than R_N effects would falsify the result. The importance of representative maximum-lift measurements compared with the expected flight value leads also to the choice of the flight idle condition for the through-flow nacelle design, because this is the engine condition for demonstrating minimum speeds in flight.

B. Engine Interference Measurements

General Introduction

Consider again Fig. 5 and the different flowfield around the engines at second-segment climb conditions. The range of mass flow ratio to be covered is windmill on one side and maximum takoff power on the other limit. The shaded area indicates aircraft speed, which lies between Mach = 0.2 and 0.3. For the engine in maximum-power condition, the freestream tube area is between 20 and 100% bigger than the inlet area. It is obvious that the simulation of such flowfield requires special test techniques, i.e., models with powered nacelles.

Figure 6 shows a selection of possible concepts. The most simple one is the "blown nacelle," which uses a faired intake and where the jet stream is simulated by pressurized air fed into the nacelle from external sources. This technique needs additional tests to determine the intake flow effect and is only practicable if intake and exit flow do not interfere with each other.

Table 1 Transition strip positions on A300 and A310 models

Fuslage	60 mm	From the nose
Pod	28 mm	From leading edge
Pylon	16 mm	Perpendicular to leading edge
Vertical tail	5%	Chord

	Task	Engine Conditions
Performance	◦ Drag	max. Power / Windmill
	◦ max. Lift	Flight Idle
Handling	◦ Control	max. Power / Windmill
	◦ Stab.	max. Power

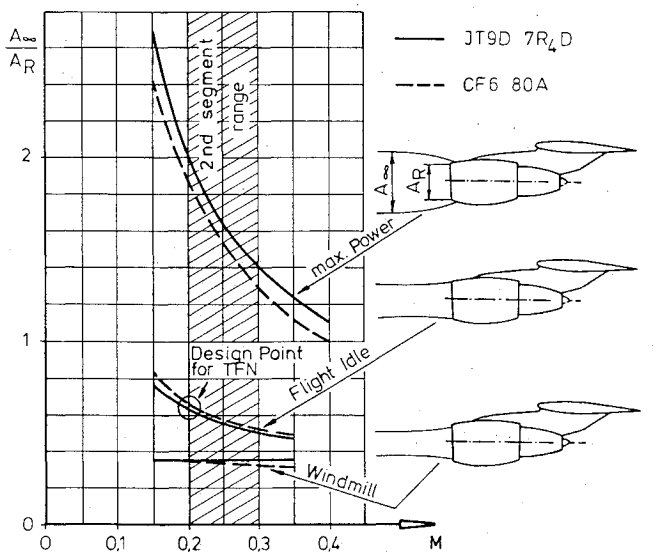

Fig. 5 Ratio of freestream tube area to propulsion highlight area.

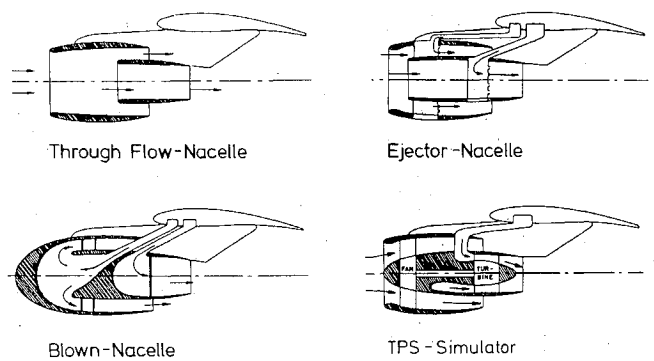

Fig. 6 Engine simulation concepts.

A step forward compared with the "blown nacelle" technique is the "ejector nacelle." This solution makes it possible to simulate intake and exit flow simultaneously but with limited accuracy. The main problems with this technique are that the intake mass flow of the ejector reaches only 50–60% of the real engine mass flow and that the nozzle exit flow is of high turbulence, which leads to a relatively quick jet decay with corresponding interference effects not comparable with the real engine behavior.

The most promising technique is the "turbine powered simulator" (TPS), which originally was used only for high-speed investigations. Since 1980, Messerschmitt-Bölkow-Blohm (MBB) has installed this technique to check engine interference effects at low speeds also. The DNW followed in 1982, with the possibility of testing complete models with two TPS running in different conditions.

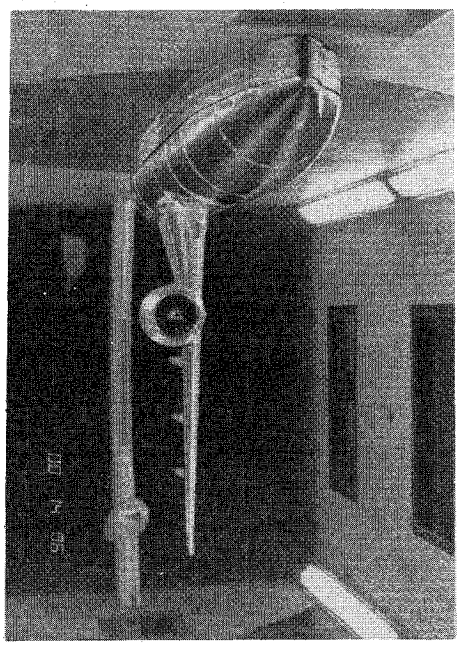

Fig. 7 A310 half-model with TPS in the MBB tunnel at Bremen.

TPS Measurements

Figure 7 shows an A310 half-model of 1/16 scale in the MBB Bremen wind tunnel. The model is fitted with a 5-in. TPS unit faced to represent CF6-80A geometry. Drive air is guided via a precise force-free air bridge through the balance into the TPS. The drive air operates a turbine that moves the fan. The advantage of this technique is a precise representation geometry, pressure ratio, and mass flow of the fan jet. Different from the real engine are the intake mass flow, temperature, and velocity of the gas generator jet efflux. However, because the hot gas part on the gross thrust of modern high-bypass engines is small and the hot jet is rounded by the fan jet, the incorrect simulation of this part is assumed to have negligible effects. For this reason, the similarity is concentrated on the fan jet, where the velocity ratio

$$\frac{V_E}{V_\infty} = \frac{\text{fan jet exit velocity}}{\text{free stream velocity}}$$

is assumed to be the standard parameter.

Attention has to be paid to the TPS intake area. Here, the mass flow is reduced by the gas generators part, where the drive air is guided direct into the turbine and therefore not passed through the intake. The reduction is approximately 14% for engines with bypass ratio of 6 : 1. Our experience is that a corresponding reduction of the TPS intake area supplied by a reshaped outer contour results in the best approach to the flow behavior of the real engine.

One severe problem arises from the fact that the thrust at low-speed conditions is higher than the aircraft drag. It is, therefore, very important to determine the TPS thrust with extremely high accuracy. For this purpose, MBB uses the calibration tank shown in Fig. 8. The balance developed for this tank has an accuracy of $\pm 0.1\%$, but it is of importance to have control units and electronic equipment to a comparable high standard. It was useful in this connection, for instance, to take the same wire arrangement for the calibration and the tunnel tests.

Evaluation of Engine Interference Drag

There are, of course, different philosophies and definitions for getting the engine interference effects. MBB uses the follow-

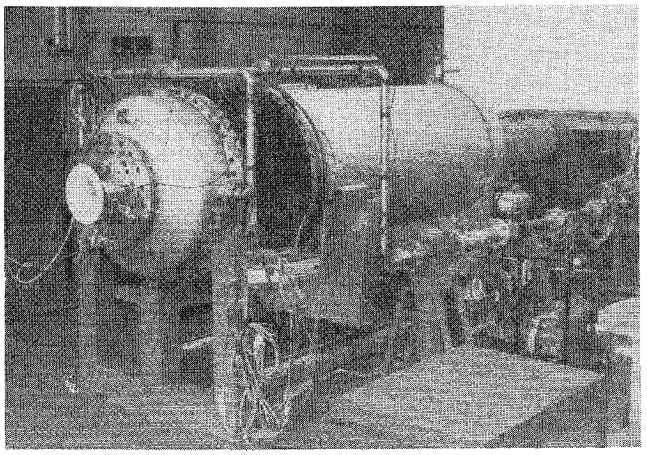

Fig. 8 MBB-TPS calibration tank.

ing approach:

Test and Analysis Procedure

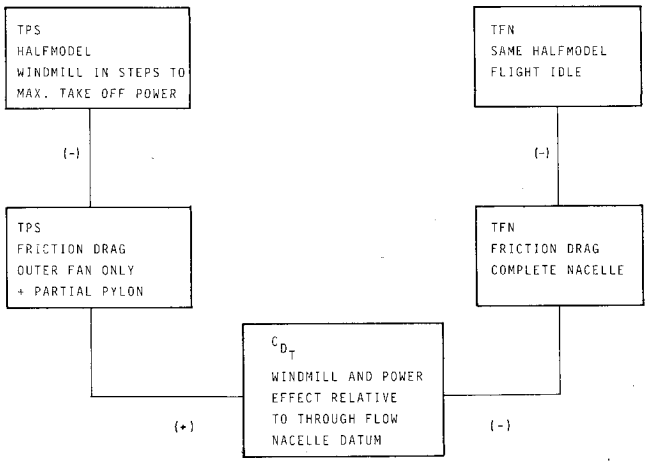

TPS thrust components in lift and drag direction are corrected in this approach, just as the internal drag portion of the through-flow nacelle, which can be determined either by theoretical calculations or extra calibration tests. The TPS thrust definition includes internal losses, the friction drag of the hot gas nozzle, and the pylon part, which is covered by the fan jet. This definition is in aggrement with the engine manufacturer. The ΔC_D values will be determined at constant-lift values.

III. Drag Scaling Procedures

A. General

After establishing the basic drag level "tail off" by the tunnel tests described before, the following corrections have to be applied to obtain final full-scale values: correction of shape drag due to Reynolds number; correction of lift-dependent drag, lift, and pitching moments due to Reynolds number; correction of thrust effects; trimming; and miscellaneous corrections.

B. Correction of Shape Drag

The lift-independent minimum-drag correction is simply the difference between model and full-scale shape drags, calculated for the respective Reynolds number:

$$\Delta C_{D_{o(R_N)}} = C_{D_{o(A/CR_N)}} - C_{D_{o(\text{Model } R_N)}}$$

The C_{D_o} values in this formula represent the sum of individual calculated shape drags for each part of the model or the aircraft, i.e., wing, fuselage, tails, etc. As usual, the shape drags are defined to be flat-plate skin friction multiplied by a shape factor:

$$C_{D_o} = C_f \cdot \frac{S_W}{S_R} \cdot \lambda$$

Skin-Friction Drag

The variation of skin friction with Reynolds number was the subject of extensive experimental investigations up to the 1960's. Several authors, e.g., Prandtl-Schlichting, Karman-Schoenherr, Schultz-Grunow etc., have developed empirical formulas derived from these data, which differ slightly in their results. For the range of interest, $2 \times 10^6 < R_N < 30 \times 10^6$, the maximum deviation of the R_N dependent drag described by these formulas is less than 0.25% of the total symmetrical drag. So, in contrast to the high-speed case where this deviation might become more important because the cruise drag coefficient is much lower, there is no special preference for one or the other equation in the low-speed takeoff case. Nevertheless, for the prediction of the fully turbulent part, MBB uses Prandtl-Schlichting, given by

$$C_{f(T)} = \frac{0.455}{(\log R_{N_C})^{2.58}}$$

where R_{N_C} is the Reynolds number based on local chord. Compressibility effects will not be considered in this speed range.

The laminar part due to the smaller Reynolds number at wind-tunnel model condition up to transitions-strips is given by the Blasius equation

$$C_{f(L)} = \frac{1.328}{\sqrt{R_{N_C}}}$$

For the aircraft, fully turbulent boundary layer is assumed on all parts.

Wing and Tailplanes

The geometry of the wing in high lift configuration is defined in Fig. 9, which also illustrates a typical wing thickness distri-

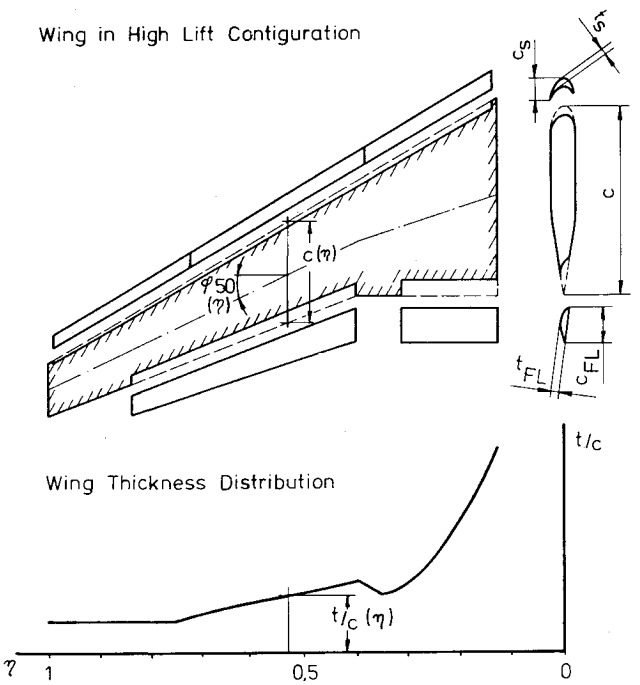

Fig. 9 Definition of wing (tailplane) dimensions.

bution. The basis is the clean wing, flaps, and flaps retracted, for which the shape drag is given by

$$C_{DoW} \cdot S_{\text{Ref}} = 4b \int_{\eta_1}^{1} C_{f(\eta)} \cdot \lambda_{(\eta)} \cdot c_{(\eta)} \cdot d_\eta$$

where S_{Ref} is the reference area, b is the half-span of the exposed wing, respectively, the tails, flaps, and slats, $C_{f(\eta)}$ is the skin-friction drag dependent on spanwise position, $\lambda_{(\eta)}$ is the shape factor dependent on spanwise position (Fig. 10), and $C_{(\eta)}$ is the wing chord. Shape factors for several wing profiles are published in Engineering Sciences Data Unit papers. A selection is given in Fig. 10 that can be applied on typical modern wing and tailplane sections. Because these shape factors are valid for the unswept case, the sweep-effect corrected value becomes

$$\lambda = (\bar{\lambda} - 1) \cos^2 \varphi_{50} + 1$$

where φ_{50} is the sweep angle of the 50% chord line.

The wing shape drag in high-lift configuration, flaps and flaps deployed, is assumed to be the clean wing value multiplied by the wetted area factor, flaps, and slat shape drags added:

$$C_{D_o \text{High Lift}} = C_{D_{oW}} \cdot \frac{S_{W\text{Rest}}}{S_{W\text{Clean}}} + C_{D_{oF}} + C_{D_{oS}}$$

where $S_{W_{\text{Rest}}}$ is the shaded area shown in Fig. 9 and $C_{D_{oF}}$, $C_{D_{oS}}$ are the shape drags of flaps and slats.

Flaps and Slats

Shape drags have to be calculated in the same way as for the wing. However, the determination of the shape factor (unswept) can be simplified to

$$\bar{\lambda} = 1 + 2.7(t/C) + 100(t/C)^4$$

For geometrical definitions, see Fig. 9.

Pods

The definition of the model through-flow nacelle geometry is shown below:

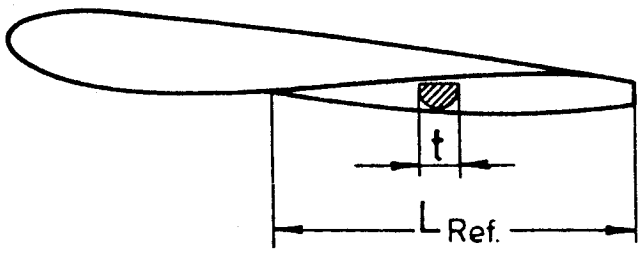

For model nacelles, it is recommended to calculate the wetted area on the basis of a mean diameter for each body. The shape factor can be determined by the equation

$$\lambda = 1 + 2.7(t/L_{\text{Ref}}) + 100(t/L_{\text{Ref}})^4$$

The pod shape drag becomes

$$C_{D_{oP}} = C_f \cdot \frac{S_W}{S_{\text{Ref}}} \cdot \lambda(\text{model})$$

For the aircraft, only the outer part of the fan cowl contributes to the aircraft drag; hence, the wetted area should be determined on the basis of the outer diameter, and the drag has to be calculated without application of a shape factor:

$$C_{D_{oP}} = C_f \cdot \frac{S_W}{S_{\text{Ref}}} (\text{aircraft})$$

where S_W is the wetted area of the fan cowl outer contour.

Pylon and Flap Track Fairings

Typical pylon and fairing geometries are shown below:

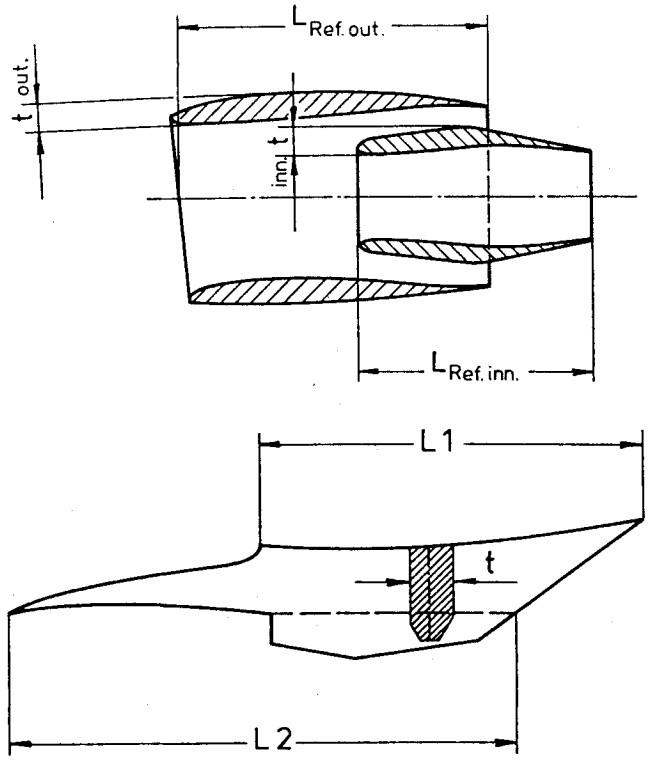

The Reynolds number to determine the skin-friction coefficients is based on L_{Ref}, which, in the case of the pylon, is a mixture of L_1 and L_2. In any case, the wetted areas are calculated to be twice the projection area. For the shape drag, the same formulas can be applied as for the model pods.

Fuselage

In the case of the A310 and A300-600, the fuselage contributes more than 30% to the total shape drag of the aircraft. It therefore plays the most important part within the C_{D_o} corrections. The calculation is similar to the other aircraft components. With the shape factor shown in Fig. 11, the fuselage drag becomes

$$C_{D_o} = C_f \cdot \frac{S_W}{S_{\text{Ref}}} \cdot \lambda$$

where the Reynolds number is referred to the complete fuselage length.

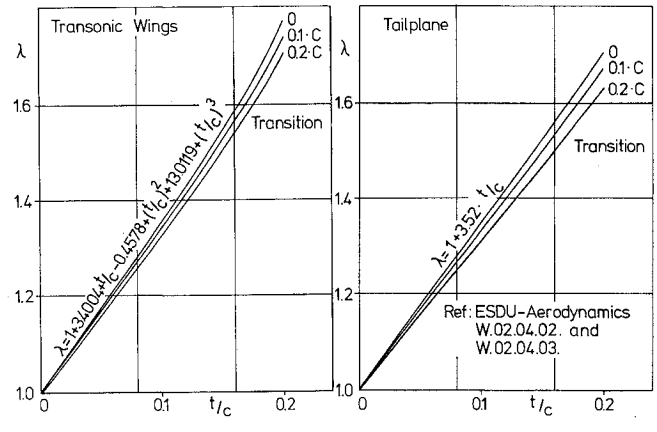

Fig. 10 Shape factors for wing and tailplane.

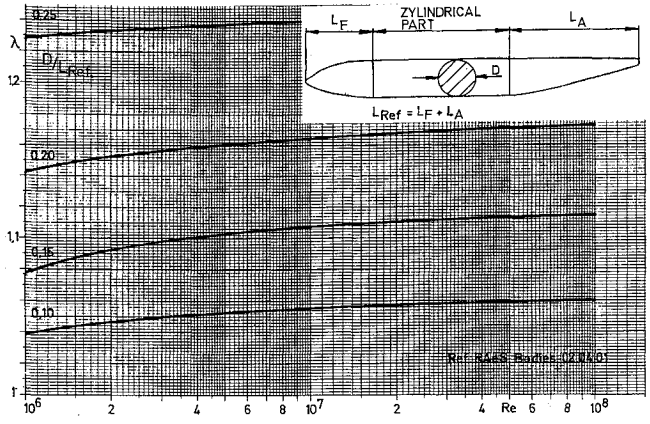

Fig. 11 Shape factors for fuselage.

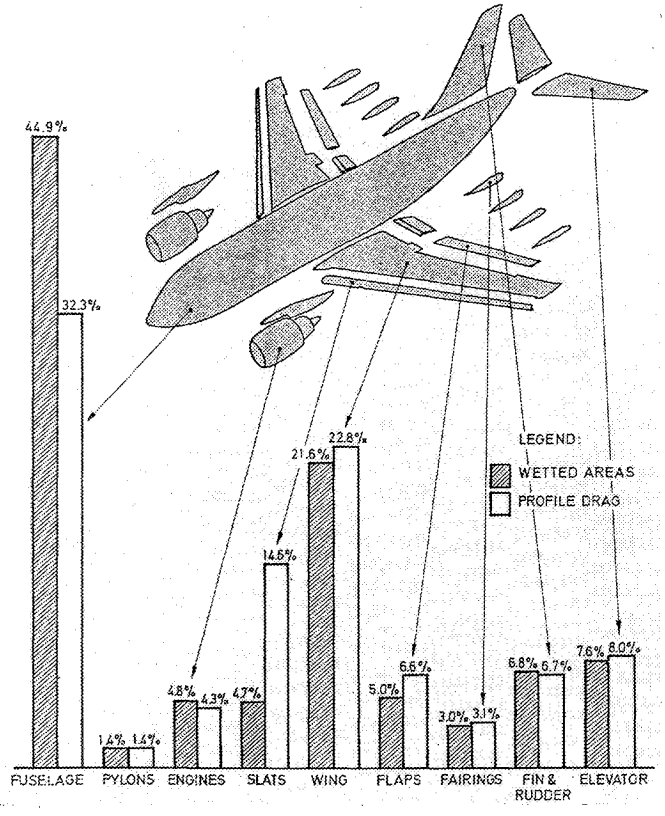

Fig. 12 Breakdown of wetted areas and shape drags, A310.

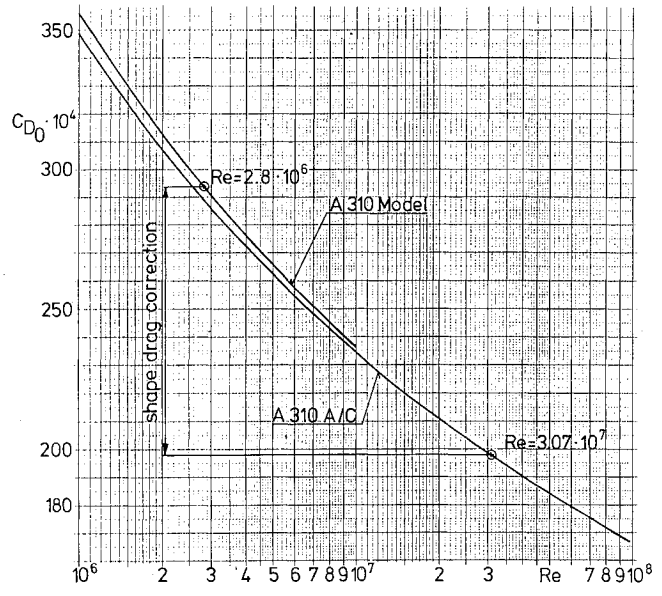

Fig. 13 Calculated shape drags for A310 model and aircraft conditions.

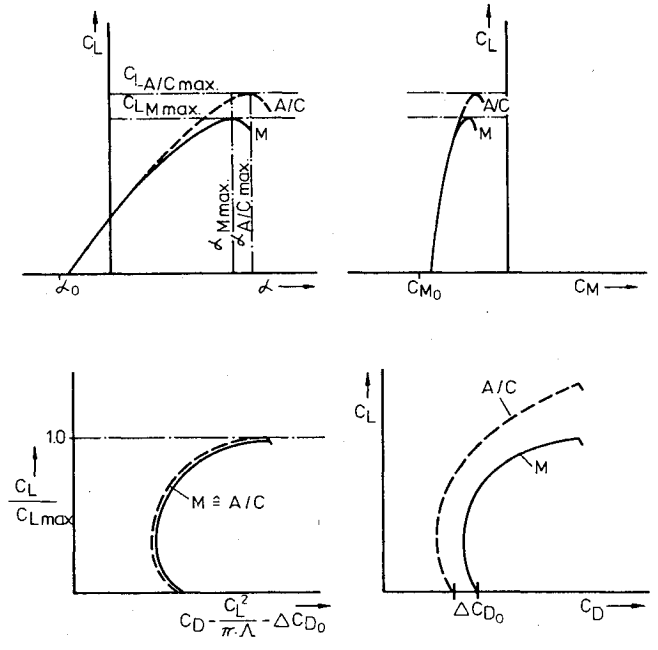

Fig. 14 Effect of Reynolds number on lift, pitching moment, and drag.

Summary Section

A summary of the calculated A310 shape drags is shown in Fig. 12. This picture demonstrates that, in general, the aircraft component drag levels are of the same order of magnitude as the wetted areas. Exceptions are the fuselage and slats. The fuselage contributes approximately 45% to the total wetted area, but the drag portion is only 32%, which indicates that, although the A310 fuselage is attributed to the wide-body family, the shape factor is relatively small compared with other components. Against that, the slats produce about 15% of drag by a wetted-area contribution of approximately 5%. With this, the slats produce after fuselage and wing the highest shape drag of all aircraft components. Figure 13 shows the calculated A310 shape drag vs Reynolds number for the aircraft and the model tested in the DNW. The discontinuous function is due to the difference in the pod drags. For the model, inner and outer parts have to be accounted for, whereas at the aircraft, only the fan cowl outer portion contributes to the aircraft drag. Flight reference and model test Reynolds number are marked in the figure. The difference between the calculated drags at these conditions is the shape drag correction to be applied on the model results. The amount is 96 drag counts, which corresponds to 7% of the total aircraft drag at a typical takeoff configuration.

C. Correction of Lift-Dependent Drag, Lift, and Pitching Moments Due to Reynolds Number

General

A general assumption for arriving at the correct drag level is that the model flow behavior is close to the expected aircraft behavior. This requirement defines a minimum test Reynolds number where no flow separation occurs in the lift range of interest (up to $C_{L_{1.2V_{smin}}}$) and where the maximum lift is controlled by same type and position of separated flow as on the aircraft. If one compares such tunnel measurements with flight tests or with tunnel results obtained at higher Reynolds num-

bers, on principle, the higher Reynolds number results show higher maximum lift at higher angles, similar but later beginning nonlinearities, and stretched polar shapes. It has been found that this behavior can be regulated. Following the assumption that the viscous effect on lift for any Reynolds number is proportional to the respective maximum lift, the general scaling law becomes

$$C_{L(A/C)} = \frac{C_{L\max(A/C)}}{C_{L\max(M)}} \cdot C_{L(M)}$$

where (A/C) denotes "aircraft" or any other reference Reynolds number and (M) model Reynolds number and test result. The unknown aircraft maximum lift has to be determined either by a combination of tunnel data and flight test results of existing aircraft or other prediction methods. Figure 14 shows the principle of the applied corrections.

Correction of Lift

As already mentioned, the lift transposition to flight is

$$C_{L(A/C)} = \frac{C_{L\max(A/C)}}{C_{L\max(M)}} \cdot C_{L(M)}$$

The lift belongs to an aircraft angle of incidence, which becomes

$$\alpha(A/C) = \frac{C_{L\max(A/C)}}{C_{L\max(M)}} [\alpha_{(M)} - \alpha_{o(M)}] + \alpha_{o(M)}$$

This equation can be derived by the assumption that zero lift angle α_o and the lift curve slope in its linear region is identical for model and aircraft conditions. Of course, this assumption is limited to moderate flap settings, where the initial aerodynamic load is comparably small.

Correction of Pitching Moments

Due to the change in maximum lift and in maximum angle of incidence, the pitching moments also have to be corrected, although the effect on trim drag is very small. With the assumption that zero pitching C_{M_o} and the slope vs lift in its linear region is identical for model and aircraft, the corrected value becomes

$$C_{M(A/C)} = \frac{C_{L\max(A/C)}}{C_{L\max(M)}} [C_{M_{(M)}} - C_{M_{o(M)}}] + C_{M_{o(M)}}$$

which is equivalent to the formula for the α correction.

Correction of Lift-Dependent Drag

The lift region of interest for which the second-segment climb drag should be properly defined lies between $C_{L(1.4V\text{smin})}$ and $C_{L(1.2V\text{smin})}$. This corresponds to lift values of 60–80% of the maximum lift (1 g). The drag in this region can be sufficiently described by the equation

$$C_D = C_{D_o} + \frac{K}{\pi \cdot A} \cdot C_L^2$$

where the lift-dependent portion $K/(\pi \cdot A)C_L^2$ consists of the induced drag $K1/(\pi \cdot A) \cdot C_L^2$ and an additional Reynolds number–dependent part C_{DC} which is the subject of the correction. In most of the cases, it is sufficient to work with the ideal induced drag ($K_1 = 1$), so that finally the Reynolds number –dependent drag portion is defined by

$$C_{DC} = C_{D_{(M)}} - C_{D_{o(M)}} - \frac{C_L^2(M)}{\pi - A}$$

This portion, obtained from model tests, is assumed to be the same for the aircraft at lift values of the same proportional distance to the maximum lift value. That means

$$C_{DC} = f\left(\frac{C_L}{C_{L\max}}\right)$$

is assumed to be independent from Reynolds number, as indicated in the bottom left sketch of Fig. 14. The final aircraft drag, untrimmed without tail, is then defined by

$$C_{D(A/C)} = C_{DC} + \Delta C_{D_{o(RN)}} + \frac{C_{L(A/C)}^2}{\pi \cdot A}$$

where $C_{D(A/C)}$ is the aircraft drag at $C_{L(A/C)}$, C_{DC} defined earlier is the drag portion at $C_{L(M)}$, which is $C_{L(A/C)} \cdot C_{L\max(M)}/C_{L\max(A/C)}$, and ΔC_{D_o} is the correction of shape drag due to Reynolds number as defined earlier. The lift-dependent drag correction term at constant lift can then be expressed by the equation

$$\Delta C_{Di(RN)} - [K(M) - 1]\left[\left(\frac{C_{L\max(M)}}{C_{L\max(A/C)}}\right)^2 - 1\right] \cdot \frac{C_L^2}{\pi \cdot A}$$

For typical takeoff lift values and a test Reynolds number 2×10^6, this part of correction results in 2–3% of the total aircraft drag.

D. Residual Drag Corrections

Trimming

The scaled wing/fuselage configuration has to be trimmed to the forward center of gravity position and for a reference gross thrust coefficient C_{T_G}. The consideration of thrust is limited to the pitching moment coefficients, whereas the thrust contribution to the aircraft lift will be regarded with the field length calculation. The drag increment due to trim at constant aircraft lift consists of the tail drag due to tail lift and the higher wing/body drag due to the lift increase, which is necessary to overcome the lift loss on the tail for balancing the wing/body pitching moment. Referring to the tail area, the tail drag portion becomes

$$C_{D_T} = \underbrace{\frac{K_T}{\pi \cdot A_T}(C_{L_T} - C_{L_{oT}})^2 \cos\varepsilon}_{\text{Tail-induced drag}} + \underbrace{C_{L_T} \sin\varepsilon}_{\text{tail thrust}}$$

Herein, the tail lift follows from the aircraft's wing/body pitching moment, including thrust contribution, in the course of which it is advisable to correct the wing/body pitching moments first to zero gross thrust (see next section) to make the coefficients independent from the designed mass flow ratio of the model nacelle. Then, assuming that the moments are referred to 25% mean aerodynamic chord (MAC), the tail lift to trim is

$$C_{LT} = \frac{\overset{1)}{C_{M(A/C)}} + \overset{2)}{(X_{c.g.}/MAC - 0.25) \cdot C_{M(A/C)}} + \overset{3)}{C_{TG}\frac{Z_A}{MAC}}}{\left(\frac{L_T - X_{c.g.}}{MAC} + 0.25\right) \cdot \frac{S_T}{S_{\text{Ref}}}}$$

where 1) is the wing/body pitching moment corrected to zero gross thrust, 2) regards the center of gravity position, and 3) is the thrust contribution (see next section). Because the so-defined trim lift is referred to the tail force system and to the tail area, the final contribution to the trimmed aircraft lift becomes

$$\Delta C_{L_{T(A/C)}} = C_{L_T} \cdot \frac{S_T}{S_{\text{Ref}}} \cdot \cos\varepsilon$$

and the drag

$$\Delta C_{D_{T(A/C)}} = C_{D_T} \cdot \frac{S_T}{S_{\text{Ref}}}$$

The total increment from wing/body to the trimmed aircraft drag at given lift is approximately

$$\Delta C_{D_{\text{Trim}}} \approx \underset{1)}{C_{D_{oT}}} + \underset{2)}{\Delta C_{D_{T(A/C)}}} - \underset{3)}{2 \cdot \frac{K_{(A/C)}}{\pi \cdot A_{(A/C)}} \Delta C_{L_{T(A/C)}} \cdot C_{L(A/C)}}$$

where 1) is the tail shape drag, including interference fuselage/tail, 2) is the tail lift-dependent drag portion to trim, and 3) is the wing/body drag contribution caused by increasing the angle of incidence to overcome the trim lift loss.

Thrust Effect

Normally the thrust is not part of the aerodynamic coefficients. An exception is the data basis for performance calculations, where the thrust contribution on pitching moment is part of the trimming procedure. It therefore indirectly influences the aircraft drag polar.

On the basis of the previous definitions and after some simplifications, the total engine contribution on the aircraft pitching moment can be derived to

$$\Delta C_{M_E} = \underset{1)}{\frac{F_G - F_R}{q \cdot S_{\text{Ref}}} \cdot \frac{Z_A}{MAC}} + \left(\underset{2)}{\frac{F_R}{q \cdot S_{\text{Ref}}}} + \underset{3)}{2 \frac{Ae}{S_{\text{Ref}}}} \right) \frac{X_A}{MAC} \cdot \alpha'$$

where 1) gross thrust (F_G) minus ram drag (F_R) mutiplied with the distance between thrust axis and center of gravity (c.g.) the net thrust portion, 2) is due to the change of inlet momentum direction, and 3) is due to the change of "apparent mass flow" momentum direction, when Ae is the exhaust engine area. On the basis of this formula, special cases can be derived, such as for the model through-flow nacelle, where in a first approach the net thrust can be assumed to be zero. Then the model pod contribution becomes

$$\Delta C_{M_P} = \left[\frac{F_R}{q \cdot S_{\text{Ref}}} + 2 \frac{A_e}{S_{\text{Ref}}} \right] \frac{X_A}{MAC} \cdot \alpha'$$

This means that the pure aerodynamic portion for the model and full-scale engines is identical if the geometry and mass flow ratio are equivalent. The effects of divergent mass flow ratios from the reference condition have to be taken from TPS measurements, as mentioned at the beginning.

In most of the cases, it is profitable to correct the model pitching moments to zero gross thrust, which is

$$\Delta\Delta C_{M_P} = -2 \left(\frac{A_\infty}{A_{\text{Ref}}} \right) \cdot \frac{A_{\text{Ref}}}{S_{\text{Ref}}} \cdot \frac{Z_A}{MAC}$$

where $A_\infty / A_{\text{Ref}}$ is the designed nacelle mass flow ratio (flight idle). If the model-based pitching moments have been corrected in that way, the full-scale thrust contribution becomes

$$\Delta C_{M_{E(A/C)}} = C_{T_G} \cdot \frac{Z_A}{MAC}$$

where C_{T_G} is the gross thrust coefficient of the running engines ($C_{T_G} = F_G / q \cdot S_{\text{Ref}}$).

Parasitics

The parasitic drag contributes to the total takeoff drag by approximately 1%. It covers those portions not represented on the model, i.e., the effects of gaps, steps, roughnesses, antennas, etc. Usually, the computation follows for a typical cruise Mach number, but the result will be adopted for low speeds, too. Here, only a short description of the applied methods shall be given.

The calculation of parasitic drag items is based largely on semiempirical methods, and in the literature there exists a wide spectrum of experimental data for excrescenses. The most important calculation methods can be summarized into two main groups. Excrescences, such as steps, gaps, holes, etc., on the aircraft surface, that are small compared with the local boundary-layer thickness ($h/\delta < 0.1$). For these, the best data reduction is:

$$\frac{C_D}{C_f} = f\left(\frac{(U_\tau \cdot h}{\nu}; M_\sigma \right)$$

where $U_\tau \cdot h/\nu$ is the local Reynolds number based on the step height and the local friction velocity, and M_δ is the local Mach number. Details are also given in Refs. 11 and 12.

For the group of relatively large excrescenses, such as antennae, drainmasts, lights, and other bodies that project far into the boundary layer or through it ($h > \delta$), a calculation method has been applied, where an "independent drag" coefficient is defined which is referred to the frontal area and an effective dynamic pressure:

$$\bar{C}_D = \frac{D}{q_{\text{eff}} S_f} = f\left(\frac{\bar{u}h}{\nu}; M_\sigma \right)$$

where the effective dynamic pressure has to be derived from a boundary-layer computation.

IV. Comparison of Scaled with Measured Drags

A. Justification of the Method by Tunnel Measurements

Figure 15 shows results of an A310 test that was carried out at a very early development stage in the pressurized National Lucht-en Ruimtevaart Laboratorium (NLR) high-speed tunnel. Plotted are lift, pitching moment, and drag coefficients measured at Mach = 0.2 and different Reynolds numbers for a typical takeoff configuration with slats and flaps deployed. The picture demonstrates the typical effect of increased Reynolds number, i.e., higher maximum lift, similar but later-beginning nonlinearities, and lower drag.

Starting from the low-Reynolds number test ($R_N = 1.7 \times 10^6$), the scaling method has been applied to estimate coefficients for the higher test Reynolds number. The result is shown by the dashed lines, which demonstrate fairly good agreement with the corresponding measurements. The diagrams of most interest are placed on the bottom of the figure. On the right-hand side, the total drags are shown where the scaled drag includes C_{D_o} and $C_D = f(C_L)$ changes. In this case, the complete correction sums up to approximately 70 drag counts, which overestimates the measured effect due to Reynolds number by approximately 10 counts.

To the left, the normalized drag is shown where the C_{D_o} difference is eliminated. This picture demonstrates how the lift-dependent correction operates. In this case, the agreement of the normalization with respect to maximum lift is excellent.

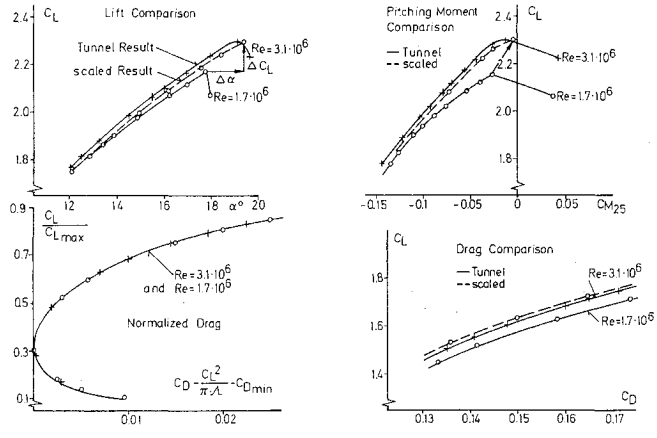

Fig. 15 Tunnel results for $R_N = 3.1 \times 10^6$ compared with scaled values based on measurements at $R_N = 1.7 \times 10^6$.

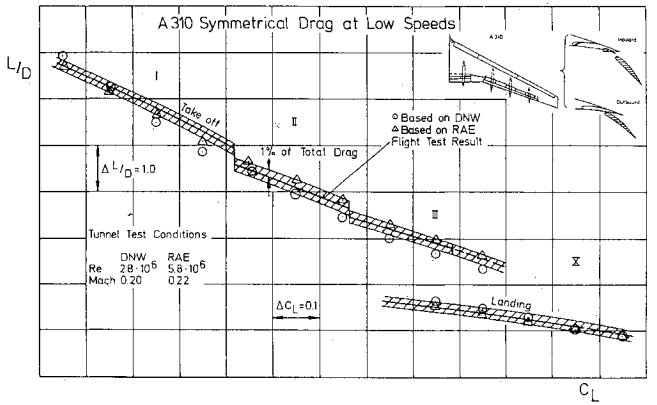

Fig. 16 Scaled drags compared with flight test results, A310.

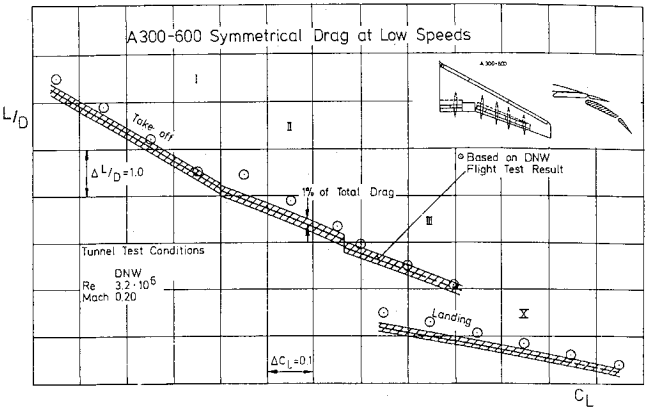

Fig. 17 Scaled drags compared with flight test results, A300-600.

However, other investigations on various projects, which were carried out since that time, show that the scatter of this correction part is in the order of $\pm 0.5\%$ for a range of Reynolds numbers between 2×10^6 and 6×10^6.

B. Comparison with Flight Test Results

Performance flight tests have been carried out by Airbus Industrie in the usual manner with individually calibrated engines. The second-segment flights were done with one engine in windmill condition as well as with both engines operating symmetrically. The drag has been calculated via a personified thrust deck and analyzed by application of a regression method. The results are shown in Fig. 16 for the A310 and in Fig. 17 for the A300-600. Both diagrams contain L/D values vs C_L for three takeoff configurations and for landing, where the marked area represents a bandwidth of $\pm 1\%$ L/D around the mean. For comparison in Fig. 16, the scaled drags based on RAE (triangles) and DNW (circles) tunnel tests are shown. The agreement is good. Only for configuration I, which is the slat out/flap in case, the mean of the scaled results lie outside the band for a small C_L region. The scaled tunnel results themselves differ less than 2% from each other. The A300-600 is aerodynamically very similar to the A300-B4. The most important differences, which nevertheless have only small effects at low speeds, are the flap system change from tabbed to simple fowler flap and the wing tip fence. Therefore, only limited low-speed tunnel tests are available for this aircraft. The scaled drag shown in Fig. 17 is based on DNW tests. Here the agreement is of less quality but still acceptable. The biggest divergence occurs for configuration II, which represents flap settings of 8 deg. It seems in this case that the basic tunnel results are less accurate. The maximum divergence is in the order of 2% L/D outside the band. This example might demonstrate that confirmation measurements in different tunnels and with various models are necessary to establish a well-proven prediction basis.

V. Conclusions

This survey has presented some of the main features of the drag scaling method used by MBB to predict the second-segment climb drag of transport aircraft. In particular, the wind-tunnel testing philosophy, the degree of engine simulation, and the corrections due to the effect of Reynolds number has been outlined. To demonstrate the overall validity of this method, tunnel and flight test results obtained with the aircraft A310 and A300-600 have been shown in comparison with the scaled values. The principal conclusions to be noted are as follows.

1) A careful model/tunnel concept is necessary to provide the basic drag and maximum lift level with the required accuracy. In particular, it has to be ensured that the model flow behavior on the wing in high-lift configuration is close to the expected aircraft flow pattern. Laminar portions of the model boundary layer have to be limited by an optimized fixation.

2) It is recommended to determine the engine installation effects by using TPS units. However, because of the complexity of this technique, the investigation should be limited to measure differences to a well-defined engine reference condition, which is "flight idle" in this case and which is represented on the basic performance model by a corresponding designed "through-flow" nacelle.

3) The quality of the determined corrections depend mainly on the accuracy of the calculated differences between model and aircraft, i.e., shape drags and maximum lifts. Therefore, the absolute levels are not so significant. This fact allows some simplifications, in particular for the calculations of wetted areas.

4) It has been demonstrated that the introduced drag estimation method is useful. A comparison with flight test result of two different transport aircraft shows acceptable agreements.